DOI: 10.19884/j.1672-5220.202404002

Preparation of Ultra-High Capacity Anode $C/SnO_2@NC@CC$ for Lithium-Ion Batteries

MOU Xina, ZHOU Xin, ASAD Khaleeq, WANG Chunrui*
College of Physics, Donghua University, Shanghai 201620, China

Abstract: SnO_2-based anodes for lithium-ion batteries (LIBs) experience volume expansion, leading to rapid capacity decay and low conductivity. To address this problem, a composite consists of C/SnO_2 with a core-shell structure and a carbonized nitrogen-doped Co-metal organic framework (Co-MOF) (NC) supported on carbon cloth (CC) was designed and prepared, which was denoted as C/SnO_2@NC@CC. C/SnO_2@NC@CC could be used directly as a flexible anode for LIBs. The combination of core-shell structure centered on carbon spheres, carbonized nitrogen-doped Co-MOF, and CC not only restricts the volume expansion but also functions as conductive networks to improve the electrical conductivity. $C/SnO_2@NC@CC$ exhibits excellent electrochemical performance with charge and discharge specific capacities of 2 066.0 and 2 077.1 mAh/g, respectively, after 120 cycles at a current density of 0.5 A/g.

Keywords: lithium-ion battery (LIB); SnO_2 anode; core-shell structure; electrode kinetics
CLC number: TM911.11 **Document code**: A
Article ID: 1672-5220(2025)04-0371-09

Open Science Identity (OSID)

0 Introduction

The need for energy storage devices with larger capacities has persisted alongside the meteoric rise in popularity of portable electronics. Lithium-ion batteries (LIBs)[1-4] are very promising electrochemical energy conversion and storage devices. They are frequently used because of their high energy density, significant potential difference, negligible memory effect, low environmental impact, and extended charging and discharging endurance. The traditional graphite anode is insufficient to fulfill the promise of the future demand for increased energy density. A variety of metals and semiconductor oxides, such as SiO_2[5-6], SnO_2[7-8], TiO_2[9] and MnO_2[10], are considered attractive options for future-generation LIBs because of their high theoretical specific capacity and cost-effectiveness. Among these candidates, the Sn-based material[11-13] is considered as one of the most ideal anodes due to the high theoretical capacity (1 494.0 mAh/g for SnO_2). During the repeated lithium insertion process, the transformation between SnO_2 and Sn is partially reversible, causing a significant volume expansion of around 200%. The formation of a solid electrolyte interface (SEI) leads to low initial coulombic efficiency (ICE). The inherent low electrical conductivity of the SnO_2 semiconductor impedes the speed of Li^+ and electron transport. As a result, significant efforts have been devoted to addressing this issue.

Currently, the most effective solutions are as follows. 1) Rational design and preparation of SnO_2-based materials with unique nanostructures[14-15]. Zhai et al.[16] designed a core-shell structured SiO_2@C-Sn/SnO_2 nanosphere, and the carbon overlayer reduced SnO_2 expansion and enhanced the electrode conductivity, while the Sn/SnO_2 doping improved the specific capacity. 2) Construction of heterostructures, especially p-n heterostructures, for developing advanced electrode materials[17-19]. Such architectures can generate synergistic effects by integrating the complementary advantages of individual components. Furthermore, incorporating carbonaceous matrices, e.g., reduced graphene oxide (rGO)[20-21] and carbon nanotube (CNT)[22-23], has been demonstrated to significantly improve electrical conductivity while mitigating anode pulverization issues. Zhan et al.[21] designed a graded ZnS/SnO_2@rGO composite material. The outer rGO matrix improved the electrical conductivity and fully alleviated the volume expansion of ZnS/SnO_2 during the cycling. Carbonaceous matrix coupling decreased ion and electron transport distances and minimized volume expansion, resulting in superior electrochemical kinetics.

To solve the problem that SnO_2 nanoparticles exhibit a large volume expansion as the number of cycles increases and are easily crushed, we design a new composite material C/SnO_2@NC@CC combining the advantages of the core-shell structure based on the

Received date: 2024-04-01
Foundation item: National Natural Science Foundation of China (No. 61376017)
* Correspondence should be addressed to WANG Chunrui, email: crwang@dhu.edu.cn
Citation: MOU X N, ZHOU X, ASAD K, et al. Preparation of ultra-high capacity anode C/SnO_2@NC@CC for lithium-ion batteries[J]. *Journal of Donghua University (English Edition)*, 2025, 42(4): 371-379.

original foundation of our group. A carbonized nitrogen-doped Co-metal organic framework (Co-MOF) (NC) grown on carbon cloth (CC) is used as a sacrificial template to create porous carbon, and glucose is employed as a carbon source to synthesize C/SnO_2@NC@CC. When C/SnO_2@NC@CC is used as the anode in LIBs, it gives high charge and discharge specific capacities of 2 066.0 and 2 077.1 mAh/g, respectively, at 0.5 A/g after 120 cycles and has superior rate performance compared to SnO_2@NC@CC.

1 Materials and Methods

1.1 Materials

Cobalt nitrate hexahydrate ($Co(NO_3)_2 \cdot 6H_2O$) was provided by Shanghai HUSHI Co., Ltd., China; 2-methylimidazole (2-MI) was provided by Adamas Beta (Shanghai) Chemical Reagents Co., Ltd., China; sodium stannate (Na_2SnO_3) was provided by Shanghai YUANYE Co., Ltd., China; glucose ($C_6H_{12}O_6$) and sucrose ($C_{12}H_{22}O_{11}$) were provided by Sinopharm Chemical Reagent Co., Ltd., China; $LiPF_6$ was provided by Canrd Co., Ltd., China. All commercially availale reagents were analytically pure and used as received without further purification.

1.2 Preparation of C/SnO_2@NC@CC, SnO_2@NC@CC and C/SnO_2

The preparation of carbonized Co-MOF on CC (C@NC@CC) was based on our group's prior research[5]. After that, 0.030 mol of $C_6H_{12}O_6$ and 0.007 mol of Na_2SnO_3 were dissolved in 50 mL of deionized water and continuously stirred for 2 h to form a clarified solution. The solution was enclosed with a 100 mL Teflon liner and maintained at 180 ℃ for 3 h to obtain a black or brown precursor. The precursor was heated under an N_2 atmosphere with a ramp rate of 5 ℃/min to 500 ℃ and annealed for 2 h. The final product was marked as C/SnO_2@NC@CC. SnO_2@NC@CC denotes the product formed when no additional carbon source was introduced in the preparation process. C/SnO_2 represents the powder product obtained when the NC and CC substrates were omitted in the preparation process.

1.3 Morphology and structure analyses

Surface morphologies of the composite materials during each preparation process were observed by a field emission scanning electron microscope (S-4800, Hitachi, Japan) and a high-resolution transmission electron microscope (JEM-ARM300F, JEOL Ltd., Japan) operated at an accelerating voltage of 200 kV. X-ray diffraction (XRD) patterns of the composite materials were tested with an X-ray diffractometer (Rigaku, Japan). X-ray photoelectron spectroscopy (XPS) data of the composite materials were obtained by using an Escalab 250Xi spectrometer (Thermo Scientific, USA) with an excitation source of Al-Kα radiation.

1.4 Electrochemical measurements

Electrochemical measurements were fulfilled on account of CR2016-type coin cells, which were prepared within a glove box filled with high-pure Ar. Lithium foil was used as a negative electrode (counter electrode). Celgard 2400 membrane was utilized to be a separator. The 1 mol/L $LiPF_6$ solution (consisting of ethylene carbonate (EC) and dimethyl carbonate (DMC) with a volume ratio of 1∶1) was utilized to be an electrolyte. Electrochemical performance was evaluated by using a Landian Battery Testing System (Model CT2001A, Wuhan Land Electronics Co., Ltd., China). Rate capability tests were conducted at varying current densities, while cycling stability was measured at a fixed current density, with a voltage window of 0.01–3.00 V. Cyclic voltammetry (CV) was obtained at a scanning rate of 0.01 mV/s, and electrochemical impedance spectroscopy (EIS) with an amplitude of 5 mV at a frequency range of 0.01 to 100.00 kHz was tested by using the CHI-660 workstation (Shanghai Chenhua Instrument Co. Ltd., China).

2 Results and Discussion

2.1 XRD and XPS analyses of C/SnO_2@NC@CC

Figure 1 displays the XRD patterns of different products in the preparation process of C/SnO_2@NC@CC. By comparing the peak positions with the powder diffraction file (PDF), it is evident that the diffraction peaks of C/SnO_2 at 2θ = 26.61°, 33.89°, 51.78°, 54.75° and 65.93° correspond to the (110), (101), (211), (220) and (301) crystal planes of tetragonal SnO_2 (PDF#41-1445), respectively. The XRD peak at approximately 26.50° corresponds to the (002) crystal plane of hexagonal graphite (PDF#41-1487), confirming that the one-step hydrothermal method successfully constructs both the graphite-like carbon framework and C/SnO_2 composite in a single process. After the introduction of CC, the XRD peaks were obscured by more intense C peaks. The XRD pattern of CC exhibits characteristic peaks at around 25.30° and 43.10°, which are consistent with the reported diffraction features of CC in Ref. [24]. In the XRD pattern of C@NC@CC, the diffraction peaks of graphitic C and CC overlapped due to their similar crystal structures, resulting in a pattern dominated by CC. By comparing the XRD pattern of C/SnO_2@NC@CC with those of the previously mentioned products, diffraction peaks similar to those of SnO_2@NC@CC can be observed. Generally, the (100) crystal plane, which has the highest surface energy, would be the most ideal for Li^+ adsorption[25]. However, it is very difficult to achieve this in practical situations. Instead, the (211) crystal plane has been identified as a favorable plane for Li^+ storage, as it exhibits a relatively high surface energy and a low energy barrier for Li^+ compared to other planes. Notably, the XRD pattern of

C/SnO_2 shows a prominent diffraction peak corresponding to the SnO_2 (211) crystal plane, which will facilitate rapid Li^+ diffusion when used as an anode material.

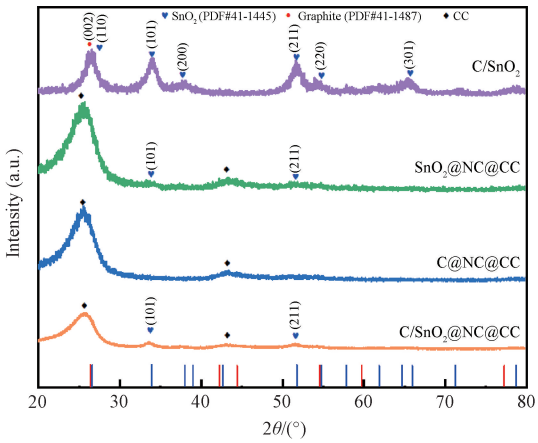

Fig. 1 XRD patterns of C/SnO_2@NC@CC, C@NC@CC, SnO_2@NC@CC and C/SnO_2

Figure 2(a) shows the XPS survey spectrum of C/SnO_2@NC@CC, revealing that the composite consists of Sn, O, C and N. The presence of N 1s peak in the XPS spectrum confirms that N is doped into the carbon framework, in agreement with the mechanism reported in Ref. [9]. Figure 2(b) presents the XPS spectrum of Sn 3d, showing double peaks at 495.7 and 487.4 eV that correspond to Sn $3d_{3/2}$ and Sn $3d_{5/2}$ of Sn^{4+}, and double peaks at 497.1 and 488.7 eV that correspond to Sn $3d_{3/2}$ and Sn $3d_{5/2}$ of Sn^{2+}[26], respectively. The presence of Sn^{2+} in SnO_2 can be attributed to the formation of oxygen defects in the crystal lattice by high-temperature calcination in an inert N_2 gas atmosphere[27]. In Fig. 2(c), the high-resolution spectrum of O 1s can be deconvoluted into two peaks. The peak at 533.3 eV suggests the presence of oxygen vacancies (O_{vac}), and the peak at 531.7 eV correspands to Sn—O[28]. Moreover, the C 1s spectrum (Fig. 2(d)) can be deconvoluted into three peaks corresponding to C—O—C (288.2 eV), C—C (286.4 eV) and Sn—C (284.7 eV)[29].

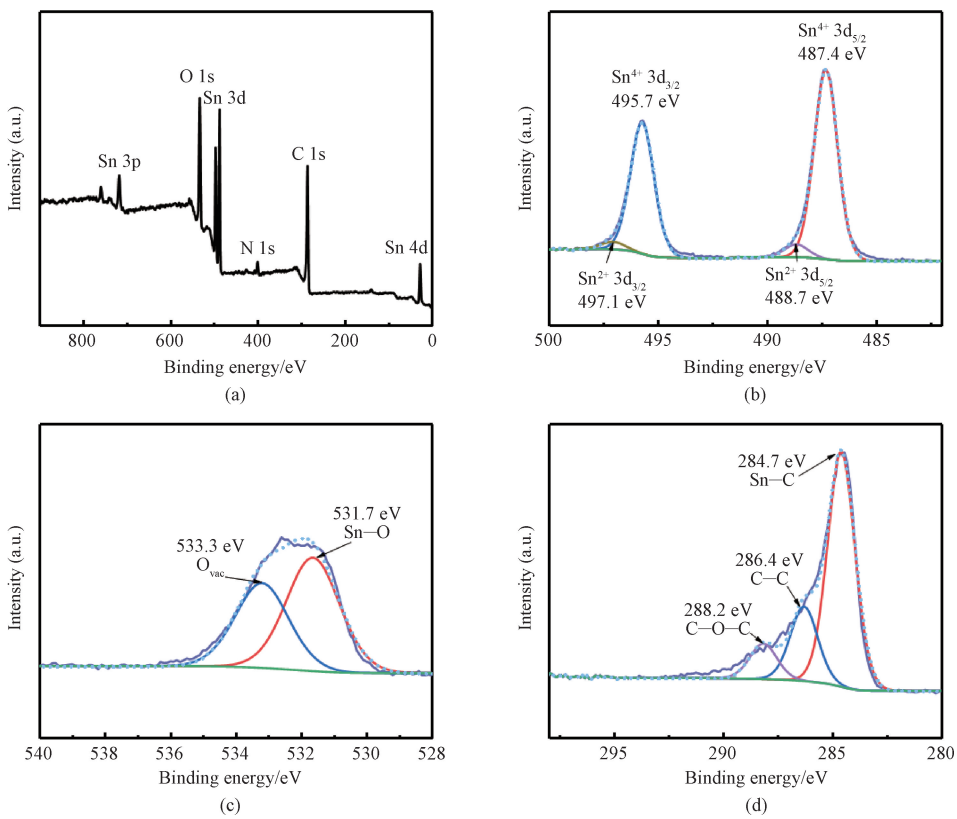

Fig. 2 XPS spectra of C/SnO_2@NC@CC: (a) survey spectrum; (b) Sn 3d; (c) O 1s; (d) C 1s

2.2 Surface morphologies of C/SnO_2@NC@CC and SnO_2@NC@CC

Figure 3(a) shows the scanning electron microscopy (SEM) image of NC@CC obtained from the previous work of our group. Figure 3(b) is the SEM image of C/SnO_2@NC@CC, where C/SnO_2 spheres are uniformly distributed on the carbonized nanosheets. As can be seen from the partial enlargement in Fig. 3(b), the diameter of C/SnO_2 is about 70–80 nm. As shown in Fig. 3(c), the transmission electron microscopy (TEM) image further illustrates the size and structure of C/SnO_2. The high-resolution TEM (HRTEM) image of C/SnO_2 (Fig. 3(d)) shows typical lattice spacings of 0.34 and 0.26 nm, corresponding to (110) and (101) planes of SnO_2, respectively. This proves that the outer layer of C/SnO_2 spheres consists of SnO_2 particles.

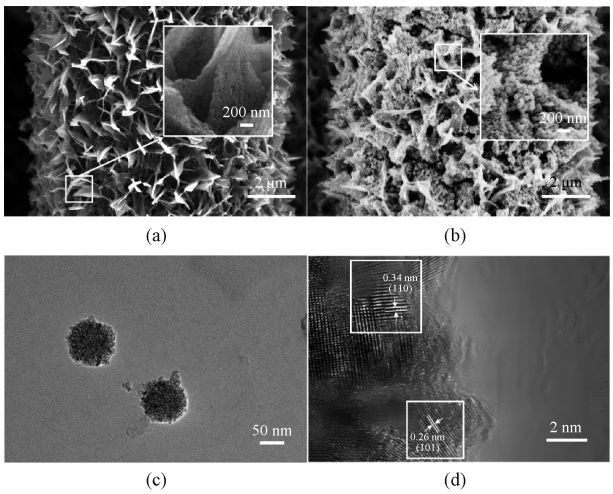

Fig. 3 Morphologies of samples: (a) SEM image of NC@CC; (b) SEM image of C/SnO_2@NC@CC; (c) TEM image of C/SnO_2@NC@CC; (d) HRTEM image of C/SnO_2@NC@CC

2.3 Electrochemical performances of C/SnO_2@NC@CC

Figure 4(a) shows the CV curves for the initial three cycles of C/SnO_2@NC@CC measured at a scanning rate of 0.1 mV/s. The CV curve for the first cycle (1st) exhibits a significantly different cathodic peak compared to the following cycles. In the first cathodic scan of C/SnO_2@NC@CC, there is a distinct cathodic peak at about 0.75 V, which is highly correlated with the decomposition of the electrolyte and the generation of the SEI[30]. In this process, SnO_2 is involved in the reaction to form Sn and Li_2O, and a large amount of Li^+ is consumed ($SnO_2+2Li^++2e^- \longrightarrow SnO+Li_2O$; $SnO+2Li^++2e^- \longrightarrow Sn+Li_2O$). This process is irreversible and a weakening of the intensity of the peak is evident during subsequent cycles. As a result, this leads to the low ICE of the material. The other sharp cathodic peak around 0.01 – 0.10 V is due to the embedding of Li^+ in the carbon skeleton and the Li_xSn alloying ($Sn+xLi^++xe^- \rightleftharpoons Li_xSn$ ($0<x\leqslant 4.4$)). It can be seen that cathodic and anodic peaks show symmetrical shapes and similar magnitudes in the CV profiles. From the second cycle (2nd), the profile of the CV curve overlapped well, indicating its high reversibility of lithium-ion intercalation and cycle stability.

Figure 4(b) shows the charge-discharge curves for the initial three cycles of C/SnO_2@NC@CC measured at a current density of 0.1 A/g. C/SnO_2@NC@CC exhibits the first cycle charge and discharge specific capacities of 2 792.5 and 3 540.1 mAh/g, respectively. The first cycle charge and discharge specific capacities of C/SnO_2@NC@CC far exceed the theoretical capacities of SnO_2. It has an ICE of around 78.8%. The reason for the relatively low ICE can be attributed to the partial irreversibility of the reaction of SnO_2 with Li^+ and the formation of the SEI. During the first cycle (Fig. 4(b)), the positions of the potential inflection points and plateaus are close to those observed in the CV curves, further demonstrating the storage behavior of Li^+. The second cycle charge and discharge specific capacities of C/SnO_2@NC@CC are 2 735.8 and 2 793.3 mAh/g, respectively, and the coulombic efficiency rises to 98%. In the second and third cycles, the charge-discharge curves of C/SnO_2@NC@CC overlap well, indicating that the C/SnO_2@NC@CC electrode has high reversibility and cycling stability.

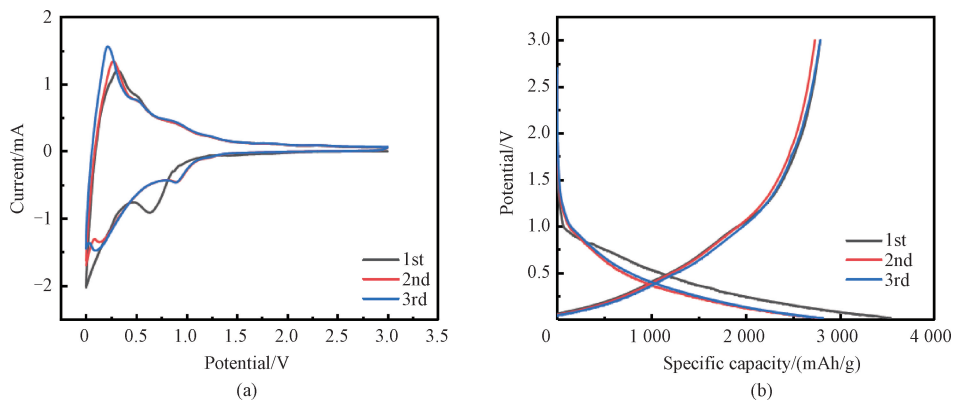

Fig. 4 Electrochemical performances of C/SnO_2@NC@CC: (a) CV curves; (b) charge-discharge curves

Figure 5(a) shows the rate performance of C/SnO_2@NC@CC and SnO_2@NC@CC at current densities of 0.1, 0.2, 0.3, 1.0, 2.0 and 3.0 A/g, and then back to 0.1 A/g. The specific capacity of C/SnO_2@NC@CC is higher than that of SnO_2@NC@CC at different current densities. At 3.0 A/g, the charge and discharge specific capacities of C/SnO_2@NC@CC still remain at 854.8 and 859.1 mAh/g, which are almost three times those of SnO_2@NC@CC (302.6 and 309.8 mAh/g). The decreased performance of C/SnO_2@NC@CC at high current density results from increased side reactions between the electrode and electrolyte. When the current density is returned to 0.1 A/g, the charge and discharge specific capacities of C/SnO_2@NC@CC can reach

2 621.8 and 2 616.6 mAh/g, respectively, suggesting that no capacity decay occurred after cycling at high current density. The enhanced capacity of C/SnO_2@NC@CC is attributed to the synergistic effect of the carbon sphere and the carbon skeleton, as high carbon content generally improves conductivity, thereby facilitating electron transfer. The carbon spheres guide the orderly distribution of SnO_2 so that the electrode material has a large specific surface area to fully contact the electrolyte. Using NC as support skeleton can suppress the volume expansion of SnO_2, thus a more uniform and stable SEI layer is formed, and the stability of the structure is maintained.

The cycle performance of C/SnO_2@NC@CC and SnO_2@NC@CC at a current density of 0.5 A/g is shown in Fig. 5(b). The initial charge and discharge specific capacities are 2 417.8 and 3090.5 mAh/g for C/SnO_2@NC@CC, and 1 253.1 and 1650.2 mAh/g for SnO_2@NC@CC. A charge and discharge specific capacities of 2 066.0 and 2 077.1 mAh/g after 120 cycles are still maintained for C/SnO_2@NC@CC, which are higher than those by using anode based on SnO_2@NC@CC. Moreover, the coulombic efficiency of C/SnO_2@NC@CC is maintained above 99.5% throughout the cycle. It is highly encouraging that the C/SnO_2@NC@CC anode sustains excellent long-term cycling stability at 0.5 A/g. This indicates that the specific capacity of C/SnO_2@NC@CC remains stable in subsequent cycles, except for the initial specific capacity loss in the first cycle, which is attributed to electrolyte decomposition and SEI film formation. Nevertheless, the specific capacity of SnO_2@NC@CC shows a steady decrease, which indicates that the addition of carbon spheres plays a positive role in electrode stability.

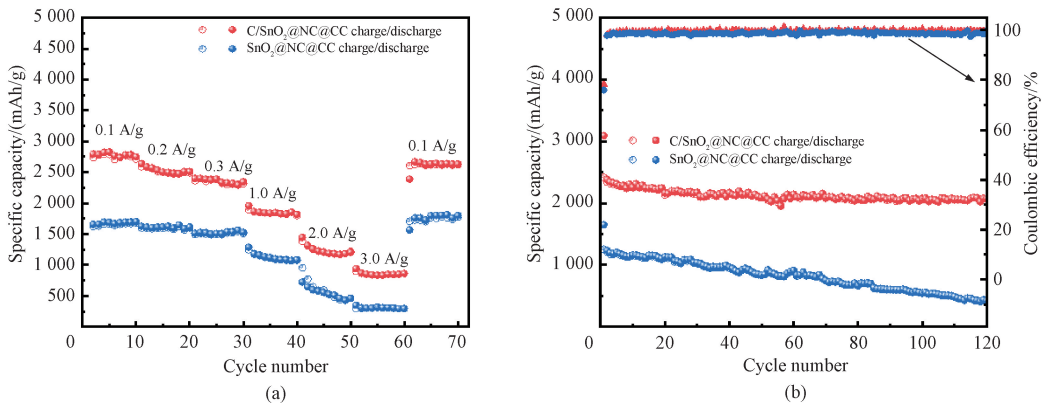

Fig. 5 Electrochemical performances of samples: (a) rate performance of C/SnO_2@NC@CC and SnO_2@NC@CC at different current densities; (b) cycle performance of C/SnO_2@NC@CC and SnO_2@NC@CC at a current density of 0.5 A/g

In this research, SnO_2 was combined with carbon from glucose and Co-MOF to obtain good electrochemical performance. There are other studies similar to this one. Hakimi et al.[31] synthesized a carbon layer by a hydrothermal method on the surface of SnO_2 nanowires (NWs). The reversible capacity of the SnO_2 NWs@C core-shell structure is 593.6 mAh/g after 100 cycles at a rate of 149.0 mA/g. Ge et al.[28] uniformly embedded ultrafine SnO_2 nanoparticles into a carbon-coated TiO_2 substrate to form a unique hybrid structure. The specific capacity of this anode remaining at 673.5 mAh/g after 250 cycles at a current density of 0.5 A/g. The addition of carbon material can provide additional electron transport paths to increase conductivity, as well as act as a support to relieve the mechanical stresses generated during the lithiation/delithiation process.

2.4 Li^+ storage kinetics of C/SnO_2@NC@CC

The kinetic performance was tested and analyzed by CV at different scanning rates[32]. From Fig. 6(a), it can be seen that the reduction peaks gradually move to lower potentials while the oxidation peaks gradually move to higher potentials as the scanning rate increases, and their intensities and widths also increase. The relationship between the currents of the reduction and oxidation peaks and their corresponding scanning rates can be expressed as

$$i = av^b, \tag{1}$$

$$\lg i = b\lg v + \lg a, \tag{2}$$

where i represents the peak current in CV; v represents the scanning rate; a and b are two constants. Determining the value of b allows a qualitative analysis of the charge storage mechanism. When $b=0.5$, the charge storage is controlled by the diffusive lithium embedding process; when $b=1.0$, the charge storage is completely controlled by the capacitance. Figure 6(b) demonstrates the relationship between $\lg v$ and $\lg i$. After calculation, the b values (slope of the fitted curves) corresponding to the reduction and oxidation processes are 0.54 (anode) and 0.53 (cathode), respectively, suggesting that the Li^+ storage mechanism in the C/SnO_2@NC@CC electrode is controlled by a combination of the two behaviors.

To further quantify the ratio between diffusion-controlled and capacitance-controlled behaviors[7], a more detailed calculation can be made according to Eqs. (3) and (4):

$$i(V) = k_1 v + k_2 v^{1/2}, \quad (3)$$

$$i(V)/v^{1/2} = k_1 v^{1/2} + k_2, \quad (4)$$

where $i(V)$ represents the current at a specific applied potential V during electrochemical testing; k_1 is the capacitance coefficient; k_2 is the diffusion coefficient; $k_1 v$ and $k_2 v^{1/2}$ denote the capacitance and diffusion control behaviors, respectively. The percentage of pseudo-capacitance contribution at different scanning rates is summarized in Fig. 6(d) according to Eqs. (3) and (4). The pseudo-capacitance contribution increases at higher scanning rates. The $C/SnO_2@NC@CC$ electrode's dominant pseudo-capacitance behavior explains its excellent cycle stability and good rate performance.

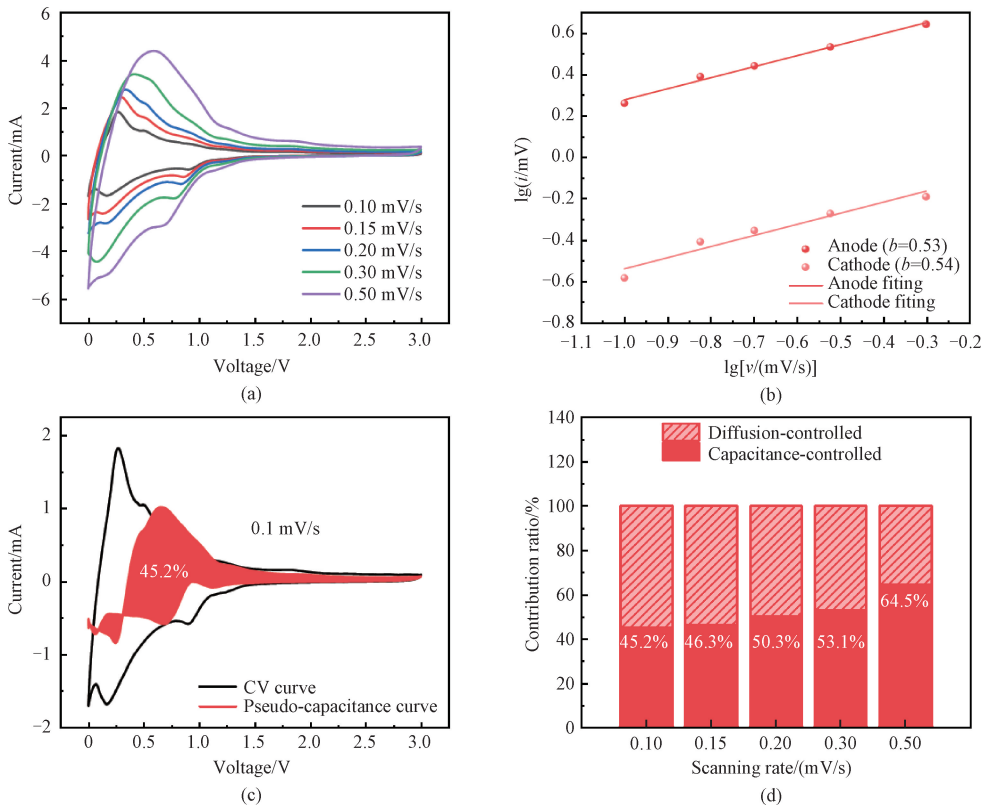

Fig. 6 Kinetic analyses of Li^+ storage: (a) CV curves of $C/SnO_2@NC@CC$ electrode at different scanning rates; (b) plot of lg i vs. lg v; (c) capacitance contribution of $C/SnO_2@NC@CC$ electrode's charge storage at a scanning rate of 0.10 mV/s; (d) contribution ratio of capacitance and diffusion-controlled charge of $C/SnO_2@NC@CC$ electrode at different scanning rates

To further study the conductivity and Li^+ diffusion in the anode of $C/SnO_2@NC@CC$, the EIS test was carried out before circulation[9]. The Nyquist plots and fitting values are shown in Fig. 7, where Z' represents the real impedance (ohmic resistance) and Z'' denotes the imaginary impedance (reactive component). The fitting values of intrinsic impedance R_s and electron transfer impedance R_{ct} are obtained based on the equivalent circuit in the inset of Fig. 7 (where W_1 represents the Warburg impedance, CPE_1 represents the constant phase element). $C/SnO_2@NC@CC$ electrodes exhibit a small intrinsic impedance ($R_s = 7.53\ \Omega$) and electron transfer impedance ($R_{ct} = 61.34\ \Omega$). These findings demonstrate that the stable SEI layer formation, the optimized electrolyte-electrode contact, and the enhanced conductivity synergistically improve the rate performance.

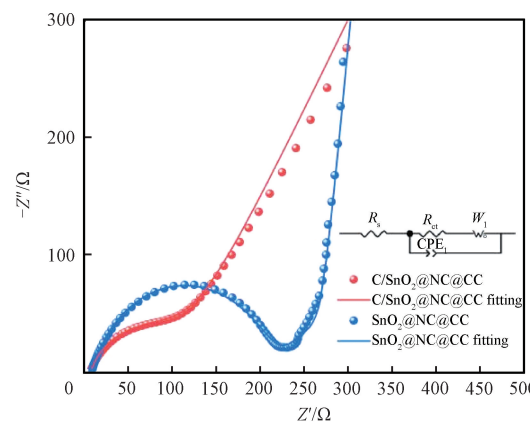

Fig. 7 Nyquist plot and equivalent circuit

2.5 Morphology of electrode after cycling

To study the volume and morphology changes of

electrode materials after cyclic use, the electrode surface of the material was characterized. As shown in Fig. 8, despite slight swelling of SnO_2 particles after cycling, their spherical morphology remains intact, with uniform distribution on NC nanosheets and no observable cracks. This stable, porous and dual-carbon structure effectively mitigates the volume expansion of SnO_2, greatly reducing the collapse and pulverization of the material structure during the cycling process, thereby exhibiting excellent electrochemical performance.

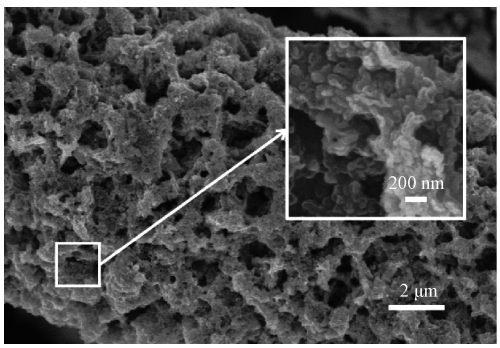

Fig. 8 SEM image of C/SnO_2@NC@CC after 120 cycles

3 Conclusions

We constructed a novel C/SnO_2@NC@CC architecture by integrating core-shell C/SnO_2 nanoparticles with CC-supported N-doped carbon derived from Co-MOF (C@NC@CC), achieving enhanced interfacial electron transfer and structural stability. C/SnO_2@NC@CC has better electrochemical properties compared to SnO_2@NC@CC with charge and discharge specific capacities of 2 066.0 and 2 077.1 mAh/g at 0.5 A/g after 120 cycles. C/SnO_2@NC@CC exhibits outstanding electrochemical performance as an LIB anode. This superiority originates from its unique hierarchical structure. Specifically, the integrated carbon spheres, CC, and Co-MOF-derived carbon frameworks collectively form an efficient conductive network. This architecture simultaneously shortens lithium-ion diffusion paths and enlarges electrolyte-active material contact areas. Consequently, the composite achieves significantly enhanced electrical conductivity. The core-shell structure centered on carbon balls, combined with carbonized Co-MOF, provides a reference for the improvement of Sn-based electrodes in lithium/sodium/potassium ion batteries and other fields.

References

[1] XU H, LI H J, WANG X M. The anode materials for lithium-ion and sodium-ion batteries based on conversion reactions: a review[J]. *ChemElectroChem*, 2023, 10(9): e202201151.

[2] DU C Y, ZHAO Z Y, LIU H, et al. The status of representative anode materials for lithium-ion batteries[J]. *The Chemical Record*, 2023, 23(5): e202300004.

[3] SHAHZAD U, MARWANI H M, SAEED M, et al. Progress and perspectives on promising covalent-organic frameworks (COFs) materials for energy storage capacity[J]. *The Chemical Record*, 2024, 24(1): e202300285.

[4] BAJWA R A, FAROOQ U, ULLAH S, et al. Metal-organic framework (MOF) attached and their derived metal oxides (Co, Cu, Zn and Fe) as anode for lithium ion battery: a review[J]. *Journal of Energy Storage*, 2023, 72: 108708.

[5] CHEN J Y, ZHOU X, ZHANG M M, et al. Designing of carbon cloth@Co-MOF@SiO_2 as superior flexible anode for lithium-ion battery[J]. *Journal of Alloys and Compounds*, 2022, 902: 163680.

[6] CHEN J Y, ZHOU X, WANG C R. One-step solution synthesis of carbon cloth @ SiO_2 composite for flexible anode of advanced lithium-ion battery[J]. *Journal of Donghua University (English Edition)*, 2022, 39(1): 22-27.

[7] LI W L, LAI H, SUN C H, et al. Heterojunction of SnO_2/Sn nanoparticles coated by graphene-like porous carbon as ultrahigh capacity anode of lithium-ion batteries[J]. *Journal of Alloys and Compounds*, 2023, 948: 169811.

[8] WANG J Y, ZHANG M M, CHEN J Y, et al. SnO_2@C/CC composite anode for lithium-ion batteries[J]. *Chemistry Letters*, 2022, 51(8): 799-802.

[9] ZHANG M M, LU A J, LI H, et al. Defective TiO_2-supported dual-Schottky heterostructure boosts fast reaction kinetics for high performance lithium-ion storage[J]. *ACS Applied Energy Materials*, 2023, 6(3): 1781-1798.

[10] VISHWANATHAN S, MOOLAYADUKKAM S, GANGAIAH V K, et al. Amorphous MnO_2-modified FeOOH ternary composite with high pseudocapacitance as anode for lithium-ion batteries[J]. *ACS Applied Energy Materials*, 2023, 6(3): 2022-2030.

[11] ZOLLER F, BÖHM D, BEIN T, et al. Tin oxide based nanomaterials and their application as anodes in lithium-ion batteries and beyond[J]. *ChemSusChem*, 2019, 12(18): 4092.

[12] KEBEDE M A. Tin oxide-based anodes for both lithium-ion and sodium-ion batteries[J]. *Current Opinion in Electrochemistry*, 2020, 21: 182-187.

[13] PONTE R, RAUWEL E, RAUWEL P. Tailoring SnO_2 defect states and structure: reviewing bottom-up approaches to control size, morphology, electronic and electrochemical properties for application in batteries[J]. *Materials*, 2023, 16(12): 4339.

[14] YANG H, ZHANG Z J, ZHAO Y W, et al. Tailoring hierarchical porous core-shell SnO_2@Cu upon Cu-Sn alloys through oxygen binding energy difference for high energy density lithium-ion storage[J]. *Journal of Physics: Energy*, 2024, 6(1): 015010.

[15] BÜRGER J C, LEE S, BÜTTNER J, et al. High-resolution nanoanalytical insights into particle formation in SnO_2/ZnO core/shell nanowire lithium-ion battery anodes[J]. *ACS Applied Materials & Interfaces*, 2023, 15(23): 28387-28397.

[16] ZHAI C Y, HE P Q, HE Y P, et al. Urchin flower-like SnO_2 nanosheets anchored on waste biomass carbon as advanced anode for lithium-ion batteries[J]. *Ceramics International*, 2024, 50(2): 3546-3555.

[17] LU Y, WANG X, KANG Q L, et al. Robust lamellar Fe_2O_3@SnO_2 heterostructure for long cycling and high-rate lithium storage[J]. *Colloids and Surfaces A: Physicochemical and Engineering Aspects*, 2023, 669: 131481.

[18] CHEN J, ZHAO N, SHI D M, et al. Superior lithium storage performance of SnO_2-modified Co_3O_4 microflowers self-assembled with porous nanosheets as anode materials in Li-ion batteries[J]. *Journal of Alloys and Compounds*, 2023, 967: 171751.

[19] DANG L Y, LI J H, YANG Y L, et al. Highly stable Fe_2O_3@SnO_2@HNCS hollow nanospheres with enhanced lithium-ion battery performance[J]. *New Journal of Chemistry*, 2023, 47(6): 3017-3025.

[20] LIU Y Y, LIU X W, ZHANG X, et al. A novel carbon microspheres @ SnO_2/reduced graphene composite as anode for lithium-ion batteries with superior cycle stability[J]. *Ceramics International*, 2022, 48(13): 18625-18634.

[21] ZHAN G H, YIN H Y, WU X H, et al. Construction of hierarchical ZnS/SnO_2@rGO heterostructures as high-performance anode materials for lithium-ion batteries by mixed-precursors strategy[J]. *Journal of Alloys and Compounds*, 2023, 968: 171906.

[22] ALAF M, ONCEL V, TOCOGLU U, et al. Synthesis and characterization of CNT@SnO_2 decorated graphene anodes for Li-ion batteries as free-standing and flexible[J]. *Journal of Materials Science*, 2023, 58(30): 12298-12311.

[23] ZHANG X Y, XIN Y, SHEN Q Y, et al. SnO_2/Cu_3Sn nanoparticles uniformly encapsulated into N-doped carbon nanofibers by electrospinning as anodes for lithium-ion batteries[J]. *Ionics*, 2023, 29(12): 5073-5084.

[24] ZHANG L H, QIN X Y, ZHAO S Q, et al. Advanced matrixes for binder-free nanostructured electrodes in lithium-ion batteries[J]. *Advanced Materials*, 2020, 32(24): 1908445.

[25] PAN L, ZHANG Y H, LU F, et al. Exposed facet engineering design of graphene-SnO_2 nanorods for ultrastable Li-ion batteries[J]. *Energy Storage Materials*, 2019, 19: 39-47.

[26] WANG X, CAO X Q, BOURGEOIS L, et al. N-doped graphene-SnO_2 sandwich paper for high-performance lithium-ion batteries[J]. *Advanced Functional Materials*, 2012, 22(13): 2682-2690.

[27] DENG X B, XU Z, LU R K, et al. The preparation of flexible graphene sponges embedded Sn nanospheres through Sn-C bonding and their improved electrochemical performances[J]. *Chemical Physics Letters*, 2022, 806: 140062.

[28] GE Q J, MA Z H, YAO M L, et al. Carbon-coated tin-titanate derived SnO_2/TiO_2 nanowires as high-performance anode for lithium-ion batteries[J]. *Journal of Colloid and Interface Science*, 2024, 661: 888-896.

[29] TANG J J, YANG J, ZHOU X Y, et al. A porous graphene/carbon nanowire hybrid with embedded SnO_2 nanocrystals for high performance lithium ion storage[J]. *Journal of Materials Chemistry A*, 2015, 3(47): 23844-23851.

[30] WU Y, WANG C, WANG C J, et al. Recent progress in SEI engineering for boosting Li metal anodes[J]. *Materials Horizons*, 2024, 11(2): 388-407.

[31] HAKIMI M, HABIBI A, SANAEE Z, et al. Implementation of binder-free SnO_2 NWs @ C electrode and LiTFSI-based electrolyte for high-performance lithium-ion battery[J]. *Journal of Physics D: Applied Physics*, 2023, 56(1): 015501.

[32] PU X J, ZHAO D, FU C L, et al. Understanding and calibration of charge storage mechanism in cyclic voltammetry curves[J]. *Angewandte Chemie International Edition*, 2021, 60(39): 21310-21318.

锂离子电池超高容量负极材料 C/SnO_2@NC@CC 的制备

牟希娜，周　鑫，ASAD Khaleeq，王春瑞*
东华大学 物理学院，上海 201620

摘　要：二氧化锡（SnO_2）基材料作为锂离子电池（lithium-ion battery，LIB）负极时会出现体积膨胀，导致容量衰减和电导率变低。针对这一问题，设计并制备了一种由核壳结构的 C/SnO_2 和氮掺杂的碳化钴金属有机框架（Co-metal organic framework，Co-MOF）（NC）负载于碳布（carbon cloth，CC）组成的复合材料，即 C/SnO_2@NC@CC。C/SnO_2@NC@CC 可直接用作锂离子电池的柔性负极。以碳球为中心的核壳结构、氮掺杂的碳化 Co-MOF 和碳布三者有机结合，一方面限制了体积的膨胀，另一方面作为导电网络提高了导电性。C/SnO_2@NC@CC 具有优异的电化学性能，在电流密度为 0.5 A/g 的条件下循环 120 次，充放电比容量分别为 2 066.0 和 2 077.1 mAh/g。

关键词：锂离子电池；SnO_2 负极；核壳结构；电极动力学